Impact of ambient oxygen on the surface structure of α-Cr_2O_3(0001)

O. Bikondoa[1,2], W. Moritz[3], X. Torrelles[4], H.J. Kim[5,6], G. Thornton[7], R. Lindsay[8]

1. *XMaS, UK-CRG , ESRF, 6 rue Jules Horowitz, F-38043 Grenoble cedex, France*
2. *Department of Physics, University of Warwick, Gibbet Hill Road, Coventry, CV4 7AL, UK*
3. *Department of Earth and Environmental Sciences, University of Munich, Theresienstrasse 41, 80333 Munich, Germany*
4. *Institut de Ciència de Materials de Barcelona (CSIC), Campus UAB, 08193 Bellaterra, Spain*
5. *ESRF, 6 rue Jules Horowitz, F-38043 Grenoble cedex, France*
6. *Department of Materials Science and Engineering and the Centre for OLED, Seoul National University, Seoul 151-744, Korea*
7. *London Centre for Nanotechnology and Department of Chemistry, University College London, 20 Gordon Street, London WC1H OAJ, UK*
8. *Corrosion and Protection Centre, School of Materials, The University of Manchester, Sackville Street, Manchester, M13 9PL, UK*

Corresponding Author:

Robert Lindsay

Tel: +44 161 306 4824

Fax: +44 161 306 4865

Email: robert.lindsay@manchester.ac.uk

Abstract

Surface X-ray diffraction has been employed to quantitatively assess the surface structure of α-Cr_2O_3(0001) as a function of oxygen partial pressure at room temperature. In ultra high vacuum, the surface is found to exhibit a partially occupied double layer of chromium atoms. At an oxygen partial pressure of $1x10^{-2}$ mbar, the surface is determined to be terminated by chromyl species (Cr=O), clearly demonstrating that the presence of oxygen can significantly influence the structure of α-Cr_2O_3(0001).

PACS numbers: 61.05.cp, 68.35.B-, 68.47.Gh, 68.43.Fg

Introduction

Fundamental experimental studies of α-Cr_2O_3(0001) are motivated both by a desire to understand the stabilization of polar oxide surfaces [1], and the importance of chromia in various applications, e.g. heterogeneous catalysis and corrosion control [2,3]. Significant nanoscale insight has already been gained from such measurements, although they have largely been restricted to ultra high vacuum (UHV). This limits their utility for mechanistic interpretation of technological performance. We address this issue here, employing surface X-ray diffraction (SXRD) [4] to elucidate the geometric structure of α-Cr_2O_3(0001) as a function of a key environmental parameter, namely the oxygen partial pressure.

α-Cr_2O_3(0001) has already been the subject of several quantitative structure determinations in UHV, using both oriented thin film [5-7] and single crystal substrates [8,9]. These studies, which are all concerned with a 1x1 surface unit cell, agree that the topmost atoms are Cr rather than O. However, their structural solutions are not identical. Refs. 5-7 favor the geometry depicted in Figure 1 (a), which is identified as Cr-O_3-Cr- on the basis of the sequence of its three topmost layers (the subscript indicates the average number of atoms in one 1x1 unit cell, which is indicated in the plan view in Figure 1 (a)). We note that Cr-O_3-Cr- is one of the three surface terminations that can be generated simply by cutting through the α-Cr_2O_3 bulk parallel to the (0001) plane; the other two are Cr-Cr-O_3- and O_3-Cr-Cr-. The geometry illustrated in Figure 1 (b), labeled $Cr_{0.70}$-O_3-$Cr^{int}_{0.30}$-, was deduced from previous SXRD measurements [8]. It is similar to the structure in Figure 1 (a), except that 30 % of the surface layer Cr atoms are in a sub-surface interstitial site (Cr^{int}). Figure 1 (c) displays a partially occupied Cr-Cr-O_3- termination, $Cr_{0.31}$-$Cr_{0.61}$-$O_{2.4}$-, which is preferred in Ref. 9.

Ab initio total energy calculations have also been undertaken to investigate the surface structure of α-Cr_2O_3(0001) [10-14]. Most pertinently, the surface termination as a function of oxygen partial pressure (chemical potential) has been predicted [12,13]. Wang and Smith [12] determine

that at around room temperature the most stable surface is O_3-Cr-Cr-, except at ultra-low O_2 partial pressures (< 10^{-40} atm). At higher temperatures other surface geometries become energetically preferred, e.g. Cr-O_3-Cr- and a chromyl (Cr=O) terminated surface (O=Cr-O_3-). In contrast, Rohrbach et al. [13] conclude that at room temperature and above the Cr-O_3-Cr- termination is thermodynamically favorable, which they attribute to the use of a more complete theoretical description. The current study provides a direct test of these *ab initio* predictions, demonstrating that a more complex surface termination needs to be considered.

Experimental Methods

Experimental work was performed on ID03 at the European Synchrotron Radiation Facility (ESRF), employing an ultra high vacuum/high pressure (UHV/HP) chamber incorporating a cylindrical beryllium window for collection of SXRD data [15]. This vessel, which had a base pressure of ~ 3 x 10^{-9} mbar, was mounted on a high precision vertical diffractometer with the α-Cr_2O_3(0001) surface in the horizontal plane. *In situ* sample preparation involved repeated cycles of Ar^+ bombardment and annealing in vacuum to approximately 1200 K. During this process, surface order was checked using the profiles of surface sensitive X-ray reflections. Exposure to O_2 was achieved by backfilling the chamber to the required partial pressure. Prior to introduction, O_2 gas underwent cryogenic distillation to minimize contaminant concentration. A mass spectrometer was used to check the purity of the O_2 admitted to the UHV/HP chamber.

SXRD data were acquired with the substrate at room temperature, using a photon energy of hν = 15.8 keV, and an incidence angle of 1º. To qualitatively follow surface geometry changes, the intensity of an X-ray reflection, namely (1, 0, 2.9), was monitored as a function of time/oxygen partial pressure. We note that this reflection was empirically selected on the basis of preliminary measurements, demonstrating that it is sensitive to changes in oxygen partial pressure. The index of this reflection, and all others hereafter, is expressed in terms of the reciprocal lattice vectors *h*, *k*, and *l*. These vectors are defined with reference to the real space (1x1) unit cell of the α-

Cr_2O_3(0001) surface, described by lattice vectors ($\mathbf{a_1}$, $\mathbf{a_2}$, $\mathbf{a_3}$) which are parallel to the [100], [010], [001] directions, respectively. The magnitudes of these lattice vector are $a_1 = a_2 = a$, and $a_3 = c$, where a = 4.957 Å and c = 13.592 Å are the bulk lattice constants [8].

For fully quantitative structure determination, a systematic series of X-ray reflections were acquired using rocking scans in which the sample is rotated about its surface normal while scattered X-ray intensity is measured. Such scans were conducted as a function of *l* at selected integer (*h*,*k*) values, and then integrated and corrected [16], to enable plots of structure factor versus perpendicular momentum transfer to be produced for crystal truncation rods (CTRs). In-plane scans in *h* and *k* at *l* = 0.5 were also undertaken to search for superstructure rods indicating surface reconstruction. No substantive evidence for such features was found.

Results

Figure 2 displays the intensity of the (1, 0, 2.9) reflection as a function of time/oxygen partial pressure. Upon exposure of the sample to an O_2 partial pressure of 5×10^{-5} mbar, there is a ~ 15 % increase in the signal, which then remains approximately constant up to 1×10^{-2} mbar. Returning to UHV did not lead to any significant change in the intensity of the (1, 0, 2.9) reflection, i.e the process is not reversible within the timeframe of the measurements. The inset in Figure 2 compares rocking scans acquired at UHV (i.e. the base pressure of the experimental chamber) and 1×10^{-2} mbar of O_2, demonstrating the significance of the variation in reflection intensity. In addition, this comparison shows that there is essentially no change in the width of the reflection, indicating that terrace size is not influenced by the presence of O_2. These data suggest that the Cr_2O_3(0001) surface geometry is modified by the presence of O_2. To validate this deduction, sets of X-ray reflections were acquired at both UHV and 1×10^{-2} mbar of O_2 to allow fully quantitative structure determinations to be performed. 335 reflections were compiled at UHV. After averaging, using P3 symmetry, these reduced to 257 non-equivalent reflections from 7 CTRs. The agreement factor between equivalent reflections was about 17 %. A smaller

dataset of 130 non-equivalent reflections from 4 CTRs was acquired at $1x10^{-2}$ mbar of O_2. We note that, as typified by the inset in Figure 2, data acquired at both UHV and $1x10^{-2}$ mbar O_2 were of comparable quality, i.e. the signal to background ratio is similar for both datasets.

For surface structure elucidation, we adopted the usual approach of generating simulated SXRD data for a potential structure, and then iteratively refining its geometry to find the best fit between experiment and theory. The ROD software [17] was used for this task. Goodness of fit was measured quantitatively by χ^2, or more strictly reduced χ^2, which is defined as follows [18]:

$$\chi^2 = \frac{1}{\mathrm{N - P}} \sum_{\mathrm{i=1}}^{\mathrm{N}} \left(\frac{\left|F_i^{\exp}(hkl)\right| - \left|F_i^{th}(hkl)\right|}{\sigma_i^{\exp}(hkl)} \right)^2 .$$

N is the number of measured structure factors, P the number of parameters optimized during fitting, and F_i^{exp}(hkl) and F_i^{th}(hkl) are the experimental and theoretically calculated structure factors, respectively. σ_i^{exp}(hkl) is the uncertainty associated with F_i^{exp}(hkl), which was calculated from comparison of equivalent reflections. χ^2 behaves such that a value of 1 indicates that experiment and theory are essentially coincident, with agreement decreasing with increasing χ^2. Values of χ^2 significantly less than 1 suggest that the magnitudes of experimental uncertainties have been overestimated**.** The quoted precision of each fitted parameter is determined by varying the parameter about its optimal value until χ^2 has increased by 1/(N-P) from its minimum value [4].

Initially, effort focused on determining the structure of the UHV surface. As a first step, mimicking the approach of Ref. 8, the three possible ideal bulk terminations, Cr-O_3-Cr-, Cr-Cr-O_3-, and O_3-Cr-Cr-, were tested. Following iterative refinement of atomic coordinates, χ^2's of 2.2, 2.0, and 2.1 were obtained for these three geometries, respectively. Given that even the smallest of these values does not represent excellent agreement, an improved solution was sought. A range of models with various geometric modifications, including fractional site

occupancy, interstitial Cr atoms, and stacking faults (i.e. lateral translation of atomic layer(s) away from location in bulk), were considered as candidates. Restricting potential solutions to those with physically reasonable inter-atomic distances, a stacking-fault-free Cr-Cr-O_3-termination with partial occupation of the three topmost Cr layers was found to provide the best match between theoretical and experimental data. A χ^2 of 1.0 was obtained for this structure, which is depicted in Figure 3 (a) and labeled $Cr_{0.22}$-$Cr_{0.31}$-O_3-. Table I lists the coordinates, fractional occupancies, and Debye-Waller factors of atoms in the optimum geometry. To arrive at this solution, 46 parameters were optimized, i.e. 35 atomic coordinates, 6 vibrational amplitudes (Debye-Waller factors), a scale factor, a surface roughness parameter (β), and 3 fractional occupancy factors. All of the non-structural parameters adopted reasonable values. We note that the surface exhibits two rotational domains due to steps, and intensities from these were averaged incoherently in the generation of simulated data [8].

Elucidation of the α-Cr_2O_3(0001) surface structure in $1x10^{-2}$ mbar O_2 commenced with refinement of the coordinates of the optimized UHV geometry. A χ^2 of 2.5 was obtained, indicating that the presence of ambient O_2 almost certainly leads to more than just surface relaxation. Following the approach for the UHV surface, a variety of alternative structures were explored in order to try to improve the agreement between experiment and theory. Structures exhibiting a significant change in surface selvedge Cr concentration were discarded as the sample was always maintained at room temperature in the presence of O_2, presumably precluding extensive Cr mobility perpendicular to the surface. The optimum geometry (χ^2 = 1.0), which is terminated by singly bound oxygen atoms (i.e. chromyl groups (Cr=O)) and labeled $O_{0.38}$=$Cr_{0.38}$-O_3-, is shown in Figure 3 (b). Removal of the chromyl oxygen increases χ^2 by 0.4, indicating that the data are sensitive to the presence of this atom. Optimum atomic coordinates, fractional occupancies, and Debye-Waller factors are listed in Table II. A total of 34 parameters were varied during structure refinement, i.e. 24 atomic coordinates, 6 vibrational amplitudes (Debye-

Waller factors), a scale factor, a surface roughness parameter (β), and 2 fractional occupancy factors (N.B. O(0) and Cr(2) fractional occupancies were constrained to be the same during structure optimization). The experimental CTRs and best-fit theoretical simulations for the UHV and 1 x 10^{-2} mbar O_2 surfaces are shown in Figures 4 (a) and (b), respectively.

Discussion

Focusing upon the UHV structure, the current solution (Figure 3 (a)) matches that emerging from quantitative low energy electron diffraction (LEED-IV) [9] (Figure 1 (c)), in that both are partially occupied Cr-Cr-O_3- terminations. However, the two structures are not quantitatively equivalent, although given that only moderate agreement between experimental and simulated data was achieved in the LEED-IV study, the agreement with the SXRD result is quite reasonable. Optimized atomic coordinates in the two studies differ, as reflected in the list of layer spacings perpendicular to the α-Cr_2O_3(0001) surface in Table III. In addition, fractional site occupancies are not identical, with lower occupation of the two uppermost chromium layers being favored in the present work, i.e. $Cr_{0.22}$-$Cr_{0.31}$- (SXRD) compared to $Cr_{0.31}$-$Cr_{0.61}$- (LEED-IV) [9]. The origin of these small, but quantitatively significant, discrepancies between the two studies may be related to the disorder in the surface. In the case of LEED-IV, vacant sites are treated approximately in the multiple scattering theory by the average *t*-matrix approximation (ATA) method [19], which is probably not sufficient for a high concentration of vacancies, such as found here. A further possibility is that the discrepancies arise from small variations in sample preparation, e.g. substrate temperature during annealing.

Turning to the central topic of this study, the impact of introducing O_2 into the ambient environment, it is evident from the optimum 1x10^{-2} mbar O_2 structure (Figure 3 (b)) that this species alters the UHV surface geometry through dissociation to form a surface chromyl (Cr=O). Previously, the Cr=O group has been reported to be present on both α-Cr_2O_3(0001) and α-

$Cr_2O_3(10\bar{1}2)$, following annealing of surfaces exposed to O_2 at low temperature [20,21]. Concurrent with the formation of Cr=O, surface chromium atoms also undergo redistribution in the presence of the O_2. Some of topmost chromium atoms of the UHV surface (Cr(1)'s in Figure 3 (a)) are apparently displaced to vacant sites in the partially occupied second chromium layer, i.e. they become Cr(2)'s in Figure 3 (b). The remaining Cr(1)'s seemingly convert into Cr(3)'s, increasing fractional occupancy of this layer from 0.70 ± 0.02 at UHV to 0.85 ± 0.01 at $1x10^{-2}$ mbar O_2. It should be noted that the total occupation of the upper chromium layers is unchanged on going from UHV to $1x10^{-2}$ mbar O_2.

Figure 5 demonstrates that in addition to altering the termination of α-$Cr_2O_3(0001)$, the introduction of oxygen also modifies near-surface substrate relaxation. Displacements away from bulk termination along the surface normal (Δz) for chromium and oxygen atoms are plotted as a function of depth into the selvedge in Figures 5 (a) and (b), respectively. As expected, the general trend of the plots is for the magnitude of Δz to diminish with depth. For the chromyl terminated surface (1×10^{-2} mbar O_2) the return to a bulk-like geometry is more rapid than the chromium terminated surface (UHV).

Concerning the energetic stability of the two optimized surface geometries, at UHV and 1×10^{-2} mbar O_2, assuming formal ionic charge states (i.e. Cr^{3+} and O^{2-}) both should be unstable due to the presence of uncompensated surface dipoles, i.e. they are both polar [1,23]. Even the presence of surface oxygen vacancies, which has not been explicitly considered in our structure optimizations due to the relatively weak X-ray scattering of oxygen atoms, would not completely quench the surface dipoles. Hence, there must be a less apparent mechanism of polarity compensation in operation. Most likely, there is a modification of the surface electronic structure, i.e. charge redistribution. More esoteric mechanisms are also possible, such as compensation through non-periodic nano-islanding as reported for ZnO(0001) [1,24].

As regards total energy calculations of the geometry of α-Cr_2O_3(0001) [10-14], none have predicted the structures deduced here. This outcome is largely a result of the theoretical work being performed on periodic slabs with small unit cells, precluding mimicry of fractionally occupied surface atomic layers. The potential pitfall of ignoring such statistical defect disorder in *ab initio* studies of oxide surfaces was presciently mentioned by Batyrev et al. in 1999 [22]. To study this lateral disorder theoretically, larger units cells, or even cluster type calculations, need to be considered. We note that of the two *ab initio* studies [12,13] examining surface structure as a function of oxygen partial pressure, Ref. 12 seemingly more closely describes the experimental results to the extent that both chromium and chromyl terminated surfaces are predicted. It should be stressed that the conclusion in this reference that the O_3-Cr-Cr- surface is the most likely geometry at room temperature does not necessarily conflict with the current UHV structure (chromium terminated) as the substrate was annealed to 1200 K during preparation prior to measurements. Chromium terminated surfaces are calculated to be stable phases at higher temperatures in Ref. 12.

Finally, it is interesting to briefly compare the results of this study to structural data obtained for the (0001) surfaces of other corundum-type metal oxide thin film and single crystal substrates. Most notably, α-Fe_2O_3(0001) and α-V_2O_3(0001) resemble α-Cr_2O_3(0001) in that it has been concluded that they too can be terminated by Metal=O groups, i.e. ferryl (Fe=O) [25,26], and vanadyl (V=O) [27,28], respectively. For α-Fe_2O_3(0001), a SXRD study analogous to the one presented here has been conducted, but as a function of temperature as well as O_2 partial pressure [25]. It reports a Fe=O termination at elevated substrate temperatures (773 K, at 10^{-6} mbar to 1 bar O_2 partial pressure). This result apparently suggests a difference between α-Fe_2O_3(0001) and α-Cr_2O_3(0001) as regards surface Metal=O formation, since we have determined that Cr=O groups form at room temperature. This apparent discrepancy probably arises from the different kinetics involved in the structural changes. For the chromia system the Cr terminated surface is oxidised to produce Cr=O, while in Ref. 25 the surface is reduced from O_3-Fe-Fe- to O=Fe-O_3- with mass transport of Fe apparently being involved. The latter reaction almost certainly involves

a greater activation energy, and so is unlikely to occur at room temperature. As regards *ab initio* predictions of the geometry of α-Fe_2O_3(0001), in contrast to their calculations for Cr_2O_3(0001) which rule out a Cr=O termination, Rohrbach et al. conclude that a Fe=O termination is favourable under strongly-oxidizing conditions [13]. Other *ab initio* calculations by Bergermayer et al. also suggest that a Fe=O terminated phase is favourable [29].

Conclusions

In summary, we have performed SXRD on α-Cr_2O_3(0001) as a function of oxygen partial pressure. We have demonstrated that the surface geometry is modified in the presence of oxygen at room temperature. A $Cr_{0.22}$-$Cr_{0.31}$-O_3- termination is determined at UHV, and a chromyl topped $O_{0.38}$=$Cr_{0.38}$-O_3- structure at an O_2 partial pressure of $1x10^{-2}$ mbar. The UHV surface geometry is largely consistent with that derived from previous LEED-IV measurements [9], although there are some small differences in atomic coordinates and fractional layer occupancies. *Ab initio* theoretical calculations performed to date [10-14] have not predicted either of the two structures.

Acknowledgements

This work was funded by grants from the EPSRC (UK), MCINN (Spain) through projects CSD2007-00041 and MAT2009-09308, and the EU.

References

1. J. Goniakowski, F. Finocchi, and C. Noguera, Rep. Prog. Phys. **71**, 016501 (2008).
2. M. Cherian, M.S. Rao, W. Yang, J. Jehng, A. Hirt, and G. Deo, Appl. Catal. A **233**, 21 (2002).
3. P. Marcus and V. Maurice, in *Passivity of Metals and Alloys*, edited by M. Schutze, Corrosion and Environmental Degradation Vol. 1 (Wiley-VCH, Weinhein, 1999).
4. R. Feidenhans'l, Surf. Sci. Rep. **10**, 105 (1989).
5. F. Rohr, M. Bäumer, H.-J. Freund, J.A. Mejias, V. Staemmler, S. Müller, L. Hammer, and K. Heinz, Surf. Sci. **372**, L291 (1997).
6. F. Rohr, M. Bäumer, H.-J. Freund, J.A. Mejias, V. Staemmler, S. Müller, L. Hammer, and K. Heinz, Surf. Sci. **389**, 391 (1997).
7. W.A.A. Priyantha and G.D. Waddill, Surf. Sci. **578**, 149 (2005).
8. Th. Gloege, H.L. Meyerheim, W. Moritz, and D. Wolf, Surf. Sci. Lett. **441**, L917 (1999).
9. M. Lübbe and W. Moritz, J. Phys. Condens. Matt. **21**, 134010 (2009).
10. C. Rehbein, N.M. Harrison, and A. Wander, Phys. Rev. B **54**, 14066 (1996).
11. J.A. Cline, A.A. Rigos, and T.A. Arias, J. Phys. Chem. B, **104**, 6195 (2000).
12. X.-G. Wang and J.R. Smith, Phys. Rev. B **68**, 201402(R) (2003).
13. A. Rohrbach, J. Hafner, and G. Kresse, Phys. Rev. B **70**, 125426 (2004).
14. S.A. Petrosyan, A.A. Rigos, and T.A. Arias, J. Phys. Chem. B **109**, 15436 (2005).
15. P. Bernard, K. Peters, J. Alvarez, and S. Ferrer, Rev. Sci. Instrum. **70**,1478 (1999).
16. E. Vlieg, J. Appl. Crystallogr. **30**, 532 (1997).
17. E. Vlieg, J. Appl. Crystallogr. **33**, 401 (2000).
18. I.K. Robinson and D. J. Tweet, Rep. Prog. Phys. **55**, 599 (1992).
19. B.L. Györffy and G.M. Stocks, in *Electronics in Disordered Metals and Metallic Surfaces*, edited by P. Phariseau, B.L. Györffy, and L. Scheire (Plenum, New York, 1979).

20. B. Dillmann, F. Rohr, O. Seiferth, G. Klivenyi, M. Bender, K. Homann, I.N. Yakovkin, D. Ehrlich, M. Bäumer, H. Kuhlenbeck, and H.-J. Freund, Faraday Discuss. **105**, 295 (1996).
21. S.C. York, M.W. Abee, and D.F. Cox, Surf. Sci. **437**, 386 (1999).
22. I. Batyrev, A. Alavi, and M.W. Finnis, Faraday Discuss. **114**, 33 (1999).
23. P.W. Tasker, J. Phys. C: Solid State Phys. **12**, 4977 (1979).
24. O. Dulub, U. Diebold, and G. Kresse, Phys. Rev. Lett. **90**, 016102 (2003).
25. C. Lemire, S. Bertarione, A. Zecchina, D. Scarano, A. Chaka, S. Shaikhutdinov, and H.-J. Freund, Phys. Rev. Lett. **94**, 166101 (2005).
26. A. Barbier, A. Stierle, N. Kasper, M.-J. Guittet, and J. Jupille, Phys. Rev. B **75**, 233406 (2007).
27. A.-C. Dupuis, M. Abu Haija, B. Richter, H. Kuhlenbeck, and H.-J. Freund, Surf. Sci. **539**, 99 (2003).
28. C. Kolczewski, K. Hermann, S. Guimond, H. Kuhlenbeck, and H.-J. Freund, Surf. Sci. **601**, 5394 (2007).
29. W. Bergermayer, H. Schweiger and E. Wimmer, Phys. Rev. B **69**, 195409 (2004).

Table I Optimized (x, y, z) coordinates of atoms comprising the UHV α-Cr_2O_3(0001) termination ($Cr_{0.22}$-$Cr_{0.31}$-O_3-) resulting from analysis of the SXRD data presented in Figure 4 (a). Fractional occupancy is indicated by a non-integer subscript in the 'Atom' column. Atomic coordinates for the bulk-terminated Cr-Cr-O_3-structure are listed. Also given are the Debye-Waller factors employed to describe vibrational amplitudes perpendicular and parallel to the surface plane**.** Figure 3 (a) provides a key to the identity of the atoms, and the axes x, y, and z. An asterisk (*) indicates that the parameter has been held constant during optimization. x and y coordinated not optimized due to symmetry constraints are italicized.

	(x, y, z) coordinates (Å)		Debye-Waller factors (Å^2)	
Atom	Bulk-terminated	Optimized	Parallel	Perpendicular
$Cr_{0.22 \pm 0.02}$(1)	3.31, 1.65, 22.65	*3.31**, *1.65**, 22.64 ± 0.04	0.5*	8.0 ± 0.7
$Cr_{0.31 \pm 0.02}$(2)	0.00, 0.00, 22.27	*0.00**, *0.00**, 22.42 ± 0.02	0.5*	8.0 ± 0.7
O(1)	1.65, 1.79, 21.33	1.53 ± 0.03, 1.53 ± 0.03, 21.12 ± 0.19	7.5 ± 1.5	0.5*
$Cr_{0.70 \pm 0.02}$(3)	1.65, 3.31, 20.39	*1.65**, *3.31**, 20.44 ± 0.01	0.5*	8.0 ± 0.7
Cr(4)	3.31, 1.65, 20.00	*3.31**, *1.65**, 20.11 ± 0.01	0.5*	8.0 ± 0.7
O(2)	1.79, 0.14, 19.06	1.68 ± 0.06, 0.15 ± 0.06, 19.47 ± 0.31	7.5 ± 1.5	0.5*
Cr(5)	0.00, 0.00, 18.12	*0.00**, *0.00**, 18.11 ± 0.01	0.5*	3.0 ± 0.4
Cr(6)	1.65, 3.31, 17.74	*1.65**, *3.31**, 17.87 ± 0.01	0.5*	3.0 ± 0.4
O(3)	1.52, 1.52, 16.80	1.53±0.03, 1.53±0.03, 16.88 ± 0.06	6.5 ± 1.4	0.5*
Cr(7)	3.31, 1.65, 15.86	*3.31**, *1.65**, 15.99 ± 0.01	3.5 ± 0.4	0.5*
Cr(8)	0.00, 0.00, 15.47	*0.00**, *0.00**, 15.59 ± 0.01	3.5 ± 0.4	0.5*
O(4)	1.65, -0.14, 14.53	1.74 ± 0.02, 0.01 ± 0.02, 14.31 ± 0.03	1.5 ± 1.0	0.5*
Cr(9)	1.65, 3.31, 13.59	*1.65**, *3.31**, 13.59 ± 0.01	0.5*	0.5*
Cr(10)	3.31, 1.65, 13.21	*3.31**, *1.65**, 13.36 ± 0.01	0.5*	0.5*
O(5)	1.79, 1.65, 12.27	1.79*, 1.65*, 12.47 ± 0.05	0.5*	0.5*
Cr(11)	0.00, 0.00, 11.33	*0.00**, *0.00**, 11.28 ± 0.01	0.5*	0.5*
Cr(12)	1.65, 3.31, 10.94	*1.65**, *3.31**, 11.03 ± 0.01	0.5*	0.5*
O(6)	1.52, 0.00, 10.00	1.52*, 0.00*, 9.81 ± 0.02	0.5*	0.5*
Cr(13)	3.31, 1.65, 9.06	*3.31**, *1.65**, 9.04 ± 0.01	0.5*	0.5*
Cr(14)	0.00, 0.00, 8.68	*0.00**, *0.00**, 8.73 ± 0.01	0.5*	0.5*
O(7)	1.65, 1.79, 7.74	1.65*, 1.79*, 7.86 ± 0.03	0.5*	0.5*
Cr(15)	1.65, 3.31, 6.80	*1.65**, *3.31**, 6.82 ± 0.01	0.5*	0.5*
Cr(16)	3.31, 1.65, 6.41	*3.31**, *1.65**, 6.52 ± 0.01	0.5*	0.5*
O(8)	1.79, 0.14, 5.47	1.79*, 0.14*, 5.51 ± 0.03	0.5*	0.5*
Cr(17)	0.00, 0.00, 4.53	*0.00**, *0.00**, 4.53 ± 0.01	0.5*	0.5*
Cr(18)	1.65, 3.31, 4.15	*1.65**, *3.31**, 4.17 ± 0.01	0.5*	0.5*
O(9)	1.52, 1.52, 3.20	1.52*, 1.52*, 3.18 ± 0.03	0.5*	0.5*

Table II Optimized (x, y, z) coordinates of atoms comprising the 1 x 10^{-2} mbar O_2 α-Cr_2O_3(0001) termination ($O_{0.38}$=$Cr_{0.38}$-O_3-) resulting from analysis of the SXRD data presented in Figure 4 (b). Fractional occupancy is indicated by a non-integer subscript in the 'Atom' column Atomic coordinates for the bulk-terminated Cr-Cr-O_3-structure are also listed. Also given are the Debye-Waller factors employed to describe vibrational amplitudes perpendicular and parallel to the surface plane. Figure 3 (b) provides a key to the identity of the atoms, and the axes x, y, and z. An asterisk (*) indicates that the parameter has been held constant during optimization. x and y coordinates not optimized due to symmetry constraints are italicized.

	(x, y, z) coordinates (Å)		Debye-Waller factors (Å^2)	
Atom	Bulk-terminated	Optimized	Parallel	Perpendicular
$O_{0.38 \pm 0.01}$(0)	N/A	*0.00**, *0.00**, 23.50 ± 0.02	0.5*	5.3 ± 0.5
$Cr_{0.38 \pm 0.01}$(2)	0.00, 0.00, 22.27	*0.00**, *0.00**, 21.93 ± 0.02	0.5*	5.3 ± 0.5
O(1)	1.65, 1.79, 21.33	1.58 ± 0.03, 1.55 ± 0.03, 21.03 ± 0.04	1.9 ± 1.1	0.5*
$Cr_{0.85 \pm 0.01}$(3)	1.65, 3.31, 20.39	*1.65**, *3.31**, 20.33 ± 0.01	0.5*	5.3 ± 0.5
Cr(4)	3.31, 1.65, 20.00	*3.31**, *1.65**, 19.99 ± 0.01	0.5*	5.3 ± 0.5
O(2)	1.79, 0.14, 19.06	1.81 ± 0.04, 0.18 ± 0.04, 19.23 ± 0.05	1.9 ± 1.1	0.5*
Cr(5)	0.00, 0.00, 18.12	*0.00**, *0.00**, 18.08 ± 0.01	0.5*	2.5 ± 0.5
Cr(6)	1.65, 3.31, 17.74	*1.65**, *3.31**, 17.70 ± 0.01	0.5*	2.5 ± 0.5
O(3)	1.52, 1.52, 16.80	1.52*, 1.52*, 16.62 ± 0.10	3.7 ± 1.7	0.5*
Cr(7)	3.31, 1.65,15.86	*3.31**, *1.65**, 15.84 ± 0.01	3.8 ± 0.8	0.5*
Cr(8)	0.00, 0.00,15.47	*0.00**, *0.00**, 15.43 ± 0.01	3.8 ± 0.8	0.5*
O(4)	1.65,-0.14,14.53	1.65*, -0.14*, 14.40 ± 0.10	1.3 ± 1.3	0.5*
Cr(9)	1.65,3.31,13.59	*1.65**, *3.31**, 13.56 ± 0.01	0.5*	0.5*
Cr(10)	3.31,1.65,13.21	*3.31**, *1.65**, 13.19 ± 0.01	0.5*	0.5*
O(5)	1.79,1.65,12.27	1.79*, 1.65*, 12.35 ± 0.06	0.5*	0.5*
Cr(11)	0.00,0.00,11.33	*0.00**, *0.00**, 11.33 ± 0.01	0.5*	0.5*
Cr(12)	1.65,3.31,10.94	*1.65**, *3.31**, 10.97 ± 0.01	0.5*	0.5*
O(6)	1.52,0.00,10.00	1.52*, 0.00*, 9.97 ± 0.07	0.5*	0.5*
Cr(13)	3.31, 1.65, 9.06	*3.31**, *1.65**, 9.08 ± 0.01	0.5*	0.5*
Cr(14)	0.00, 0.00, 8.68	*0.00**, *0.00**, 8.66 ± 0.01	0.5*	0.5*
O(7)	1.65, 1.79, 7.74	1.65*, 1.79*, 7.75 ± 0.05	0.5*	0.5*
Cr(15)	1.65, 3.31, 6.80	Not optimized	0.5*	0.5*
Cr(16)	3.31, 1.65, 6.41	Not optimized	0.5*	0.5*
O(8)	1.79, 0.14, 5.47	Not optimized	0.5*	0.5*
Cr(17)	0.00, 0.00, 4.53	Not optimized	0.5*	0.5*
Cr(18)	1.65, 3.31, 4.15	Not optimized	0.5*	0.5*
O(9)	1.52, 1.52, 3.20	Not optimized	0.5*	0.5*

Table III Comparison of atomic layer spacings perpendicular to the α-Cr_2O_3(0001) surface (Δz) derived from both LEED-IV [9] and the current UHV SXRD measurements. Bulk terminated interlayer distances are also listed. Figure 3 indicates the identity of the atomic layers.

		Δz (Å)	
Atomic Layers	Bulk-terminated	LEED-IV [9] (UHV)	SXRD (UHV)
Cr(1)/Cr(2)	0.38	0.27	0.22 ± 0.04
Cr(2)/O(1)	0.94	1.04	1.30 ± 0.03
O(1)/Cr(3)	0.94	0.96	0.68 ± 0.03
Cr(3)/Cr(4)	0.38	0.38	0.33 ± 0.01
Cr(4)/O(2)	0.94	0.93	0.64 ± 0.01
O(2)/Cr(5)	0.94	Not optimized	1.36 ± 0.01

Figure Captions

Figure 1 (Color online) Schematic models of the α-Cr_2O_3(0001)(1x1) structures emerging from UHV structure determinations [5-9]. To the left (right) are side (plan) views. Larger (smaller) spheres are oxygen (chromium) atoms. (a) displays the structure determined in Refs. 5-7, (b) and (c) are those favoured in Refs. 8 and 9, respectively. As regards atom labels, the subscript indicates the degree of fractional occupation, i.e. $Cr^{int}_{0.30}$ indicates a chromium atom located in an interstitial site with 30% occupancy. The 1x1 surface unit cell is indicated in the plan view in Figure 1(a).

Figure 2 Plot of the intensity of the (1, 0, 2.9) reflection as a function of time/oxygen partial pressure (mbar). Inset shows (1, 0, 2.9) rocking scans acquired at UHV (bold line) and 1 x 10^{-2} mbar of O_2 (thin line).

Figure 3 (Color online) Schematic models of the UHV (a) and 1 x 10^{-2} mbar O_2 (b) α-Cr_2O_3(0001)(1x1) structures determined in this study. At the bottom (top) are side (plan) views. Larger (smaller) spheres are oxygen (chromium) atoms. The numerical labelling of the atoms is employed for identification purposes. Please note '=' in the heading for Figure 3 (b) indicates the presence of chromyl (Cr=O) in this structure.

Figure 4 (Color online) Comparison of experimental CTR data (solid markers with error bars) and theoretical best-fit simulations (solid red lines). (a) and (b) show experimental data acquired at UHV and 1x10^{-2} mbar O_2, respectively. Also included in (b) are theoretically simulated data (broken blue line) for the optimum UHV geometry.

Figure 5 (Color online) Plots of chromium (a) and oxygen (b) atom displacements away from bulk termination along the surface normal (Δz) as a function of depth into the selvedge. The displacements are derived from the optimum UHV (red circles) and $1x10^{-2}$ mbar O_2 (blue squares) structures listed in Tables I and II, respectively. The numbers on the x-axes refer to the labels in Figure 3. A negative Δz indicates that the atom moves towards the bulk. The errors associated with these displacements can be obtained from Tables I and II.

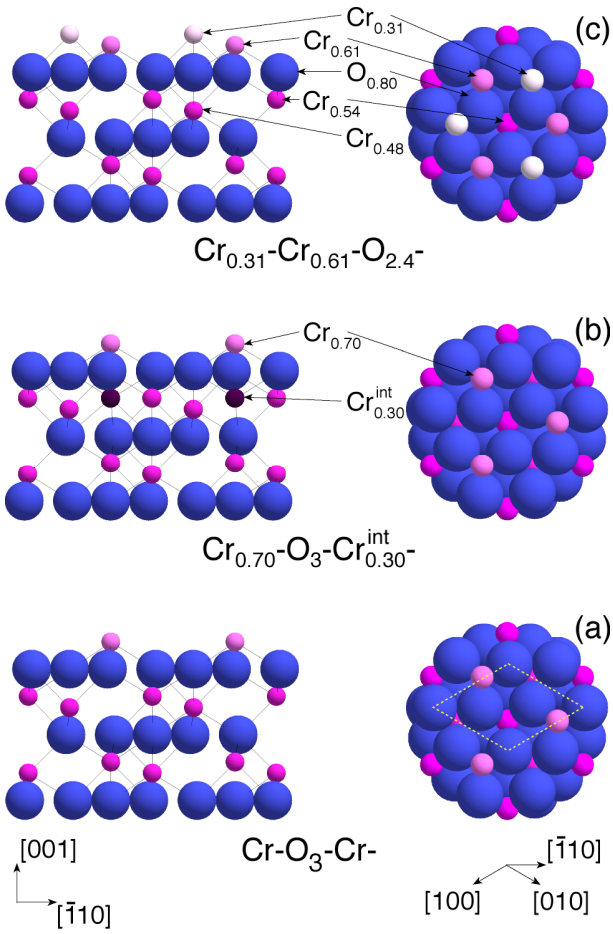
Cr0.31
Cr0.61
O0.80
Cr0.54
Cr0.48
(c)
Cr0.31-Cr0.61-O2.4-
Cr0.70
Cr0.30int
(b)
Cr0.70-O3-Cr0.30int-
(a)
[001]
[1̄10]
Cr-O3-Cr-
[1̄10]
[100]
[010]

Figure 1

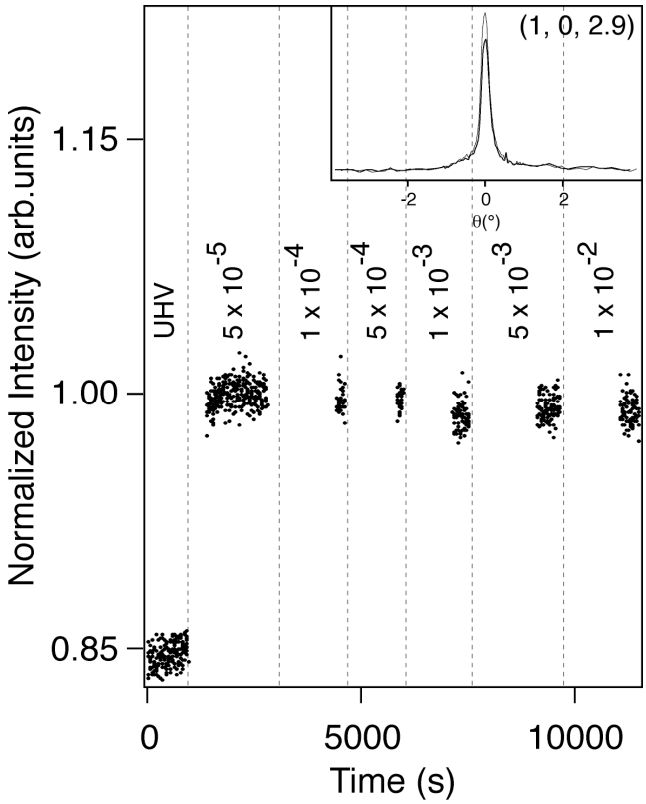
(1, 0, 2.9)
-2
0
2
θ(°)
Normalized Intensity (arb.units)
1.15
1.00
0.85
UHV
5 x 10-5
1 x 10-4
5 x 10-4
1 x 10-3
5 x 10-3
1 x 10-2
0
5000
10000
Time (s)

Figure 2

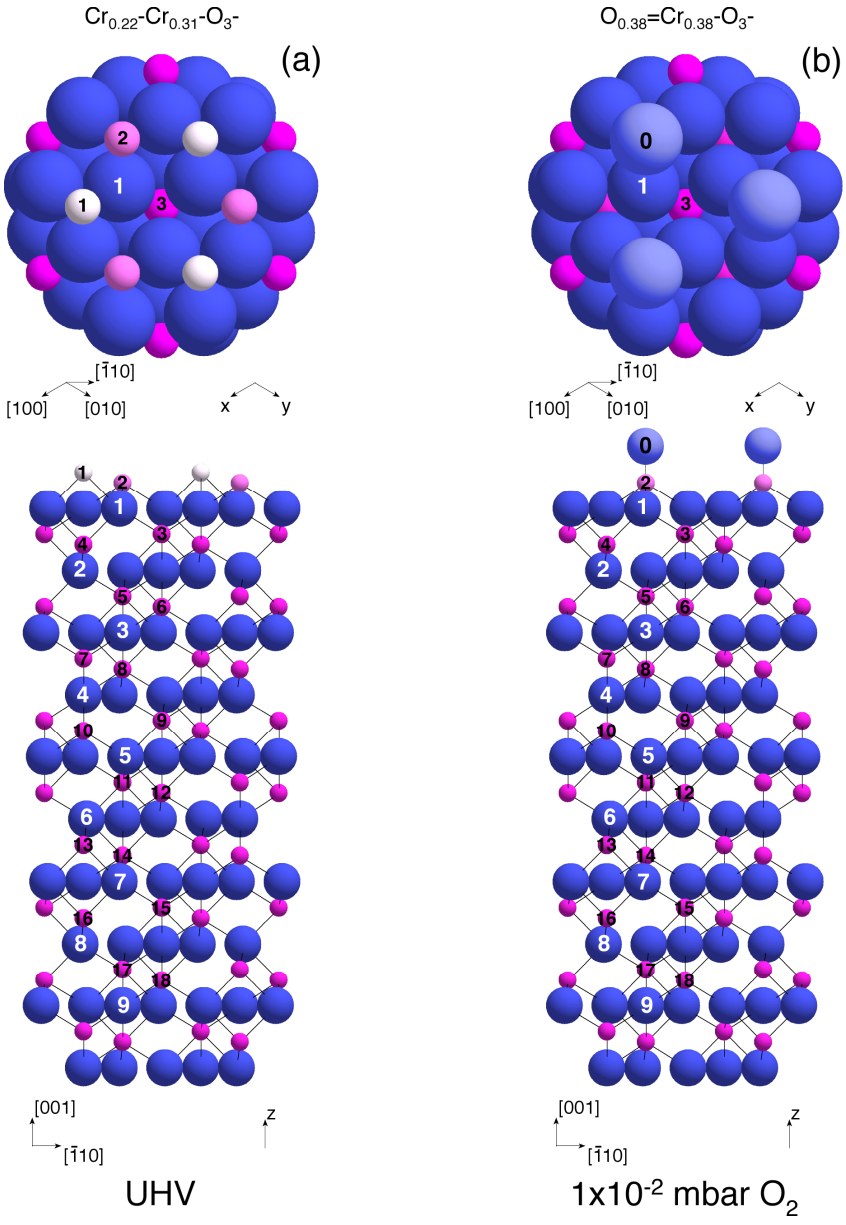
$Cr_{0.22}$-$Cr_{0.31}$-O_3-
(a)
$O_{0.38}$=$Cr_{0.38}$-O_3-
(b)
[$\bar{1}$10]
[100]
[010]
x
y
[001]
z
UHV
1x10^{-2} mbar O_2

Figure 3

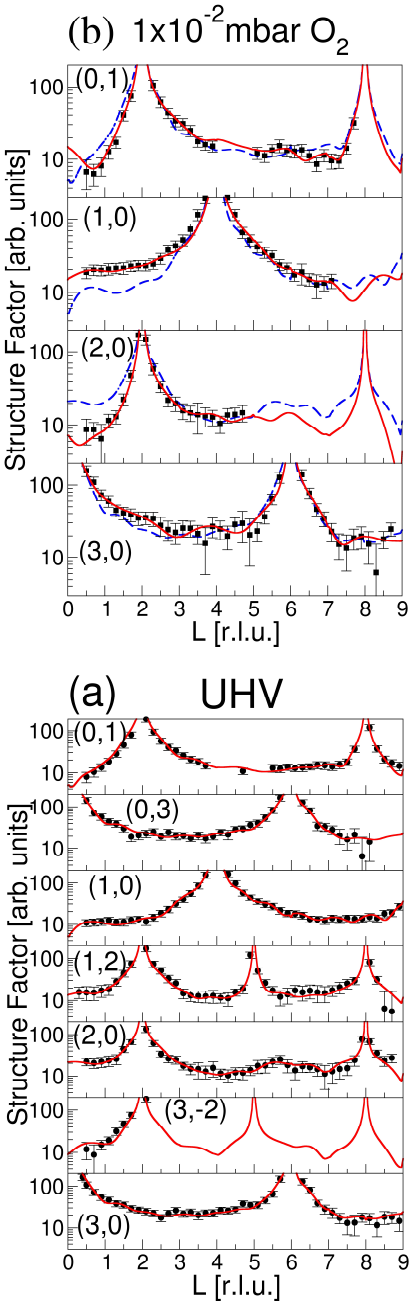
(b) 1x10^-2 mbar O2
(0,1)
(1,0)
(2,0)
(3,0)
Structure Factor [arb. units]
L [r.l.u.]
(a) UHV
(0,1)
(0,3)
(1,0)
(1,2)
(2,0)
(3,-2)
(3,0)
Structure Factor [arb. units]
L [r.l.u.]

Figure 4

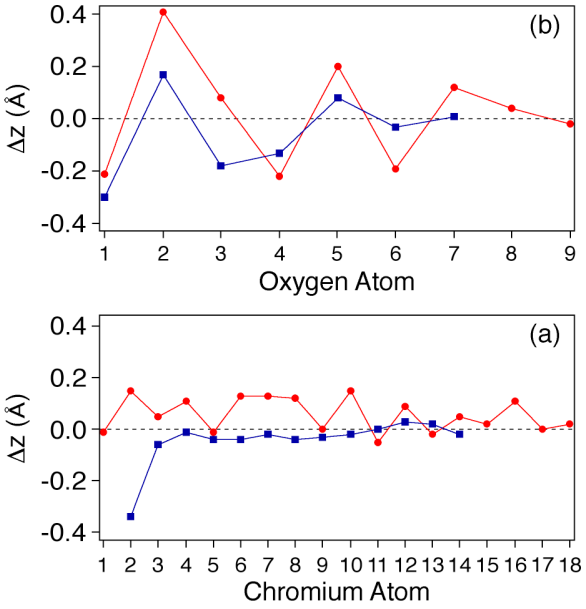
(b)
Δz (Å)
0.4
0.2
0.0
-0.2
-0.4
1 2 3 4 5 6 7 8 9
Oxygen Atom
(a)
Δz (Å)
0.4
0.2
0.0
-0.2
-0.4
1 2 3 4 5 6 7 8 9 10 11 12 13 14 15 16 17 18
Chromium Atom

Figure 5